Journal of
Materials Chemistry B

Materials for biology and medicine

Accepted Manuscript

Journal of
Materials Chemistry B

Materials for biology and medicine

rsc.li/materials-b

Volume 6
Number 3
21 January 2018
Pages 341-528

ISSN 2050-750X

ROYAL SOCIETY OF CHEMISTRY

PAPER
Wei Wei, Guanghui Ma et al
Macrophage responses to the physical burden of cell-sized particles

This is an Accepted Manuscript, which has been through the Royal Society of Chemistry peer review process and has been accepted for publication.

Accepted Manuscripts are published online shortly after acceptance, before technical editing, formatting and proof reading. Using this free service, authors can make their results available to the community, in citable form, before we publish the edited article. We will replace this Accepted Manuscript with the edited and formatted Advance Article as soon as it is available.

You can find more information about Accepted Manuscripts in the Information for Authors.

ROYAL SOCIETY OF CHEMISTRY

rsc.li/materials-b

Adipose derived Mesenchymal Stem Cell-Seeded Regenerated Silk Fibroin Reverse Liver Fibrosis in Mice

*Weilong Li [a, ‡], Xiaonan Shi [a, ‡], Daxu Zhang [b], Jingjing Hu [a], Shuo Zhao [a], Shujun Ye [a], Jingyi Wang [a], Xiaojiao Liu [c], Qian Zhang [d], Zhanbo Wang [e, *], Yaopeng Zhang [c, *], Li Yan [a, *]*

[a] The Second Medical Center and National Clinical Research Center of Geriatric Diseases, Chinese PLA General Hospital, Beijing 100853, PR China.

[b] Faculty and Institute of Hepato-Pancreato-Biliary Surgery, First Medical Center, Chinese PLA General Hospital, Beijing 100853, PR China.

[c] State Key Laboratory for Modification of Chemical Fibers and Polymer Materials, College of Materials Science and Engineering, Shanghai Engineering Research Center of Nano-Biomaterials and Regenerative Medicine, Donghua University, Shanghai, 201620, PR China.

[d] School of nursing, Lanzhou University, Gansu 730000, PR China.

[e] Department of Pathology, Chinese PLA General Hospital, Beijing 100853, PR China.

16   **ABSTRACT**

17   Liver fibrosis (LF) is an important process in the progression of chronic liver disease to

18   cirrhosis. We have previously demonstrated that RSF+ADSCs can repair acute liver injury. In this

19   study, we established a chronic LF animal model using carbon tetrachloride (CCl_4) and a high-fat

20   diet. We then investigated the liver repair capacity after transplanting RSF+ADSCs scaffolds and

21   RSF scaffolds onto the liver surface of mice. Compared with the control group, the concentrations

22   of ALT and AST in the serum were significantly reduced in the RSF and RSF+ADSCs groups.

23   HE staining and Masson trichrome staining revealed a decrease in the SAF score in both the RSF

24   and RSF+ADSCs groups. Meanwhile, the biomarkers of blood vessels and bile ducts, such as

25   CD34, ERG, muc1, and CK19, were significantly elevated in the RSF+ADSCs group. Finally,

26   transcriptome analysis showed that the *PPAR* signaling pathway, which inhibits liver fibrosis, was

27   significantly upregulated in both the RSF and RSF+ADSCs groups. Our study suggests that,

28   compared with RSF scaffolds alone, RSF+ADSCs have a significant repair effect on chronic LF

29   in mice.

30   **Keywords:** Adipose-derived stem cells (ADSCs); Regenerated Silk Fibroin (RSF); Liver Fibrosis

31   (LF); Chronic Liver Injury

32

33   **1. INTRODUCTION**

34   Currently, the global prevalence of fatty liver disease exceeds 30% [1, 2]. In China, the number of

35   people with severe fatty liver disease has reached approximately 36 million, and these individuals

36 are at risk of liver fibrosis (LF)[3]. Without effective intervention, patients with liver fibrosis may

37 face the risk of progression to cirrhosis or even liver cancer. At present, once liver fibrosis

38 progresses to cirrhosis, there are no effective drugs available. Therefore, reversing the progression

39 of liver fibrosis is crucial.

40 In recent years, stem cell regeneration research has provided new insights for treating liver

41 fibrosis[4-6]. Recent studies have shown that stem cells can promote liver regeneration through

42 transdifferentiation or paracrine mechanisms[7]. In some clinical trials, stem cells have been used to

43 treat hepatitis B-related cirrhosis. However, issues such as the difficulty in controlling stem cell

44 quality, poor stem cell engraftment capacity, and tumorigenicity make the therapeutic effects

45 unpredictable[4, 8, 9]. Fortunately, if stem cells are combined with biomaterials that can mimic the

46 liver microenvironment, their potential to promote liver fibrosis repair can be greatly enhanced[10].

47 Our preliminary studies suggest that the combination of RSF and ADSCs can effectively repair

48 liver damage[11, 12]. Additionally, we have observed the presence of vascular structures in RSF[12],

49 though their characteristics need further validation.

50 In this study, we explored the role of RSF+ADSCs in reversing liver fibrosis and their effect

51 on the formation of blood vessels and bile ducts. First, we established a liver fibrosis animal model

52 with carbon tetrachloride and a high-fat diet. Subsequently, we transplanted RSF and RSF+ADSCs

53 scaffolds onto the liver surface of the animal model. On the 7th, 14th, 30th, and 60th days after

54 transplantation, we observed the recovery of liver function. With the help of HE staining, we

55 discovered good compatibility between the scaffold and the liver. Furthermore, the result of

56 Masson ' s trichrome staining showed that RSF+ADSCs could reverse liver fibrosis.

57   Immunohistochemical staining helped us to confirm the formation of blood vessels and bile ducts.

58   Finally, according to transcriptome analysis, the molecules related to the inhibition of liver fibrosis

59   (*PPAR* signaling pathway), including *Acad1*, *Cpt1a*, *Dbi*, *Ppar*, and *Slc27a5* genes, were

60   upregulated in both RSF and RSF+ADSCs scaffold groups. We performed quantitative validation

61   using PCR technology. The results suggest that inducing the formation of blood vessels and bile

62   ducts through RSF+ADSCs to promote liver repair and reverse liver fibrosis may become an

63   alternative therapeutic method for liver fibrosis.

64

65   ## 2. MATERIALS AND METHODS

66   ### 2.1   Preparation of Electrospun RSF Matrices.

67   Based on the literature[13], the RSF matrix was prepared from all aqueous solutions. In short,

68   *Bombyx mori* silkworm cocoons were degummed and subsequently dissolved in a 9.0 M aqueous

69   solution of LiBr. The solution was diluted, centrifuged, and filtered, then dialyzed in deionized

70   water to remove salts. Finally, a 33% RSF aqueous solution was obtained by forced air cooling.

71   Using conventional electrospinning technology, RSF mats were prepared on an aluminum

72   collection plate with an electric potential of 20 kV, a flow rate of 1.2 mL/h, and a span of 10

73   centimeters between the sample and the spinneret. Then, the obtained mat with a thickness of

74   130μm was soaked in a 90 vol% ethanol aqueous solution for 30 minutes to convert the RSF to an

75   insoluble state in water.

76   ### 2.2   Cell Culture Assay

77   After collecting adipose tissue from the inguinal region of mice, it is transferred to Dulbecco's

78   modified Eagle medium (DMEM) containing antibiotics (100 mg/mL penicillin and 100 mg/mL

79   streptomycin), 2 mM Glutamax under sterile conditions. The adipose layer is cleaned with

80   phosphate-buffered saline (PBS). Then, these small pieces are digested with 15 mL of 0.2%

81   collagenase type 1 at 37°C for 2 hours. DMEM containing 10% fetal bovine serum (FBS) is

82   combined with terminate the collagenase activity, and the cells are centrifuged at 400×g for 10

83   minutes to separate the floating cells from the vascular matrix. The pellet is resuspended in

84   complete medium containing 10% FBS, 5% penicillin/streptomycin, and 1% glutamax, and passed

85   through a 100 μm nylon mesh filter to remove undigested tissue. The filtered cells are carefully

86   transferred to a 50 mL tube containing 1.077 g/mL Percoll, and subjected to density gradient

87   centrifugation at 400×g for 30 minutes. Enriched cells are collected from the interface, washed

88   twice with serum-free medium. Finally, the pellet is resuspended in DMEM containing 10% FBS,

89   100 mg/mL penicillin/streptomycin, and 2 mM Glutamax, and cultured in an incubator at 25°C

90   with 5% CO_2/95% air and 90% relative humidity. The medium is changed every 24 hours for the

91   first 3 days to remove non-adherent hematopoietic cells, and then changed every 3 days. After the

92   adherent mesenchymal stem cells reach confluence, they are digested with 0.25% trypsin-EDTA,

93   and transferred to new 25 cm² culture flasks for further culture. All experiments are performed

94   using mesenchymal stem cells after three to six passages. Ultimately, these cells are seeded onto

95   RSF scaffolds.

96   ## 2.3   Cell Induction

97   The sterilized bioscaffolds were placed in 24-well culture plates (Corning, USA). Then, $1 \times$

98   10^6 ADSCs were seeded into each 3D-PSFS. The ADSCs were cultured at 37°C with 5% CO_2.

99   Once the ADSCs adhered to 3D-PSFS, basic medium (DMEM with 10% FBS) was replaced with

100   hepatocyte induction medium which has been used in our previous research[14]. Then, 1.5 mL of

101   hepatocyte induction medium was added to each well of the 24-well culture plate and replaced

102   every 48 hours.

2.4   Animal model construction

104   All animal experiments were approved by the Institutional Animal Care and Use Committee

105   of the Chinese People's Liberation Army General Hospital. Mice aged three days were utilized to

106   prepare mesenchymal stem cells, and 6 to 8 weeks were used for animal experiments. To establish

107   a chronic LF animal model, 6- to 8-week-old mice were intraperitoneally injected with an olive oil

108   solution containing 40% CCl_4 at a dose of 2 mL/kg, three times a week. They were also fed a high-

109   fat diet containing 60% fat for 6 to 8 weeks.

2.5   Transplantation and sample collection

111   All surgeries were performed by the same surgeon. Mice were rendered anesthetized through

112   an intraperitoneal injection of pentobarbital (1%, 50 mg per kg). Exposure of the left lateral lobe

113   of the liver, and the scaffold was sutured in place. Standard layered closure of the wound was

114   performed. Mouse survival was recorded and monitored for 60 days post-transplantation. Liver

115   tissue and blood samples were obtained on the 7th, 14th, 30th, and 60th days after transplantation

116   for subsequent experimental analysis. n = 3 mice per group.

2.6   Evaluation of Liver Function and C-Reactive Protein (CRP)

118   On days 7, 14, 30, and 60 post-transplantation, serum levels of Alanine Aminotransferase

119 (ALT), Aspartate Transferase (AST), Alkaline Phosphatase (ALP), Albumin (ALB), Total

120 Bilirubin (TBIL), Triglycerides (TG), Total Cholesterol (TC), and CRP were measured using an

121 automated analyzer (Mindray, BS-240 Vet).

2.7   Histological staining and scoring

123   The collected liver tissue was fixed in 4% paraformaldehyde for 24 hours to obtain paraffin

124 sections. Following embedding, sections were cut into 6 μm slices using a Leica SM2000R

125 microtome. HE staining, as well as Masson's trichrome staining, was carried out following the

126 manufacturer's instructions (Solarbio, n=3).

127   Histological scoring was conducted using the SAF scoring system: hepatocyte steatosis was

128 scored from 0 to 3, ballooning degeneration from 0 to 2, inflammation from 0 to 2, and fibrosis

129 from 0 to 4. The fibrosis scoring follows the same criteria as the European SAF and American

130 NAS scoring systems. When fibrosis is graded as F1, it is further categorized into F1a, F1b, and

131 F1c. The total SAF score is obtained by summing the individual scores.

2.8   Immunohistochemical Staining

133   The frozen liver tissue sections were rehydrated and fixed with 4% PFA. After peroxidase

134 treatment, the sections were blocked with PBS containing 5% goat serum and 2% BSA. Then the

135 sections were incubated with primary antibodies, including anti-CD34 (Abcam), anti-ERG

136 (Abcam), anti-MUC1 (Abcam), and keratin 17/19 (cell signaling) overnight at 4℃. Secondary

137 antibodies were applied for 1 hour at room temperature. The sections were then incubated with

138 3,3'-diaminobenzidine and retained with hematoxylin. Finally, the sections were coverslipped with

139 xylene and neutral resin. Images were taken with a microscope (Nikon, Japan). n = 3 samples in

140 each group.

2.9   Reverse Transcription Polymerase Chain Reaction

142 After 7 days of transplanting the material, the liver of the mouse was lysed using Trizol

143 Reagent (from Invitrogen Life Technologies). The RNA was then reverse-transcribed into cDNA

144 under the following conditions: 50 ℃ for 15 minutes and 85 ℃ for 5 seconds. After the synthesis

145 of cDNA, it was stored at 4 ℃ before being used for real-time quantitative PCR. The PCR reaction

146 conditions were set as follows: pre-denaturation at 95 ℃ for 30 seconds, annealing at 95 ℃ for 10

147 seconds, and extension at 60 ℃ for 30 seconds, with a total of 40 cycles. Three replicate wells

148 were set, with *actin* as the internal reference, and the relative expression level was calculated using

149 the $2^{-\Delta\Delta Ct}$ method. To verify the expression levels of *CPt1a*, *Dbi*, *Ppar*, *Slc27a5*, *Tnfrsf1a*, and

150 *Tnfrsf1b* genes in liver tissue. The sequences for the primers used are listed in Supplementary

151 Table.

2.10 mRNA Transcriptome Sequencing Analysis

153 Collect liver tissue samples after 7 days, immediately freeze them and store them in a -80℃

154 refrigerator. Use TRIzol reagent or a commercial RNA extraction kit to extract total RNA, and

155 detect the concentration, purity, and integrity of the RNA using a NanoDrop spectrophotometer

156 and Bioanalyzer. Then, enrich mRNA using poly(A) selection or ribosomal RNA depletion,

157 followed by reverse transcription to synthesize cDNA and library preparation, which includes

158 fragmentation of the cDNA, end repair, addition of an A-tail, and ligation of adapters. Finally,

159 perform PCR amplification and purification. Perform high-throughput sequencing on the Illumina

160　NovaSeq 6000 or HiSeq 4000 platform, selecting the appropriate read length and sequencing depth.

161　Evaluate the quality of the raw data using FastQC, filter the data using Trimmomatic or Cutadapt,

162　and align the filtered reads to the reference genome using HISAT2 or STAR. Calculate gene

163　expression levels using HTSeq or featureCounts, and perform differential expression gene analysis

164　using DESeq2 or edgeR. Finally, perform functional annotation and pathway enrichment analysis

165　of the differentially expressed genes through databases such as GO and KEGG.

166　### 2.11 Statistical Analysis

167　Statistical analysis of two groups of parameter data was performed using the Student's t-test.

168　Normality tests were conducted, and all analyses were carried out using GraphPad Prism 9

169　software. Data are reported as mean ± standard deviation, with significance defined as a p-value <

170　0.05.

171

172　## 3. RESULTS

173　### 3.1 Construction of Liver Fibrosis Animal Model

174
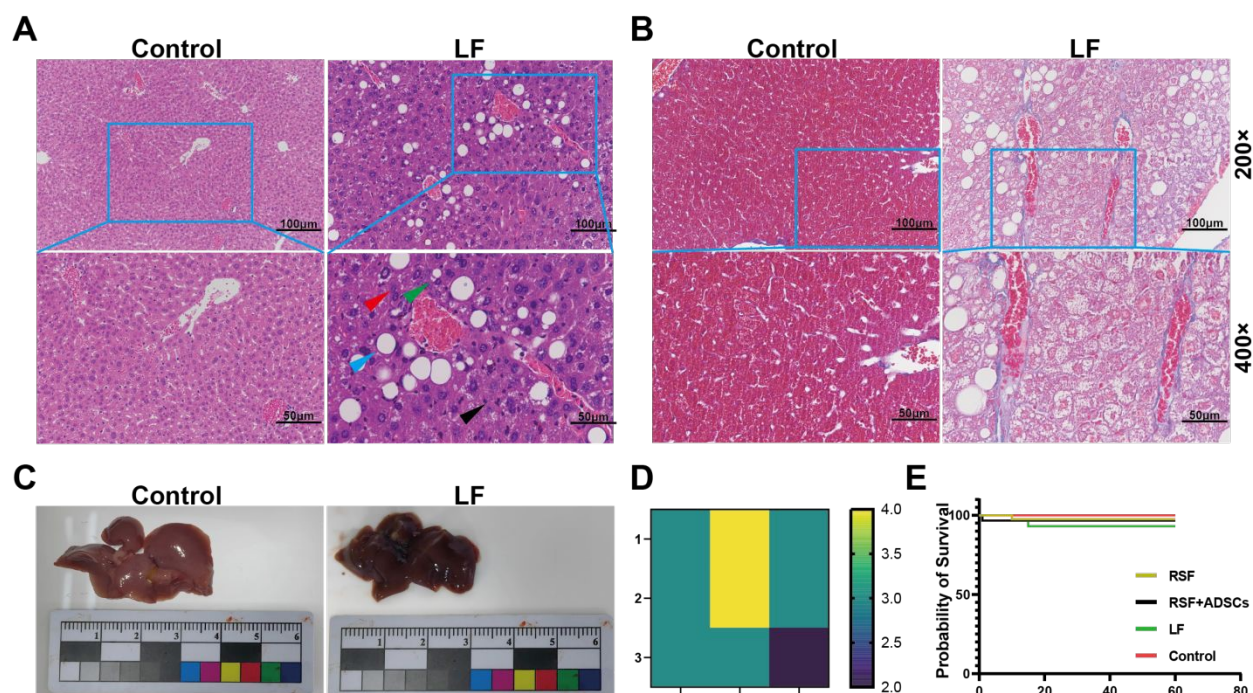
Fig.1. Construction of liver fibrosis mouse model by intraperitoneal injection of CCl₄ combined

with high-fat diet. (A)HE staining of the Control group and the LF group.(green arrows: fatty

degeneration of hepatocytes; red arrows: hydropic degeneration of hepatocytes; black arrows:

inflammatory cells; blue arrows: macrovesicular steatosis). (B)Masson staining of the Control

group and the LF group. (C)Gross liver images of normal liver versus liver after 8 weeks of

combined intraperitoneal injection of CCl₄ with a high-fat diet. (D)SAF scores. n=3. (E)Survival

rate of mice in each group after transplantation. n=3.

We constructed a mouse model of LF using intraperitoneal injection of CCl₄ combined with

a high-fat diet. After constructing the LF mouse model through intraperitoneal injection of CCl₄

combined with a high-fat diet, we transplanted either a regenerated silk fibroin scaffold loaded

with adipose-derived stem cells (RSF+ADSCs) or a pure regenerated silk fibroin scaffold onto the

liver surface of the fibrotic mice. Upon macroscopic inspection, the liver surface of mice in the

10

187 control group appeared bright red and smooth. In contrast, the liver surface of mice, after 8 weeks

188 of intraperitoneal injection of CCl_4 combined with a high-fat diet, appeared dull (Fig. 1C). We

189 performed Masson and HE staining (Fig. 1A, B) on the liver tissues of the mice to determine the

190 progression of fibrosis: After eight weeks, the normal lobular structure of the liver had disappeared.

191 We observed excessive lipid droplet accumulation, ballooning degeneration, hepatocyte swelling

192 and necrosis, and extensive inflammatory cell infiltration. Under Masson staining, the density and

193 coverage of collagen fibers (stained blue or dark blue) were significantly higher than in the normal

194 group. This resulted in dense fiber bundles or clusters, forming a complex "chicken wire" network

195 structure. The SAF score reached 10 (Fig. 1D), indicating significant fibrosis characteristics in the

196 liver by the eighth week. All of the above pathological diagnoses have been evaluated by pathology

197 specialists to ensure accuracy and reliability. The survival rates of the RSF+ADSCs group

198 compared to the control groups (LF or Control) in mice showed no significant differences at

199 various time points (P>0.05). At the endpoint of the experiment (day 60), the survival rate of the

200 RSF+ADSCs group was 97% ($\pm$2%), the RSF group was 98% ($\pm$2)%，and the LF group was

201 95% ($\pm$4%). The differences were not statistically significant (P = 0.339)(Fig. 1E). This suggests

202 that neither RSF+ADSCs nor RSF had a significant impact on the survival rate of mice after

203 transplantation.

204

205 **3.2 Biocompatibility and Degradation of RSF+ADSCs and RSF on Liver Surface**

206
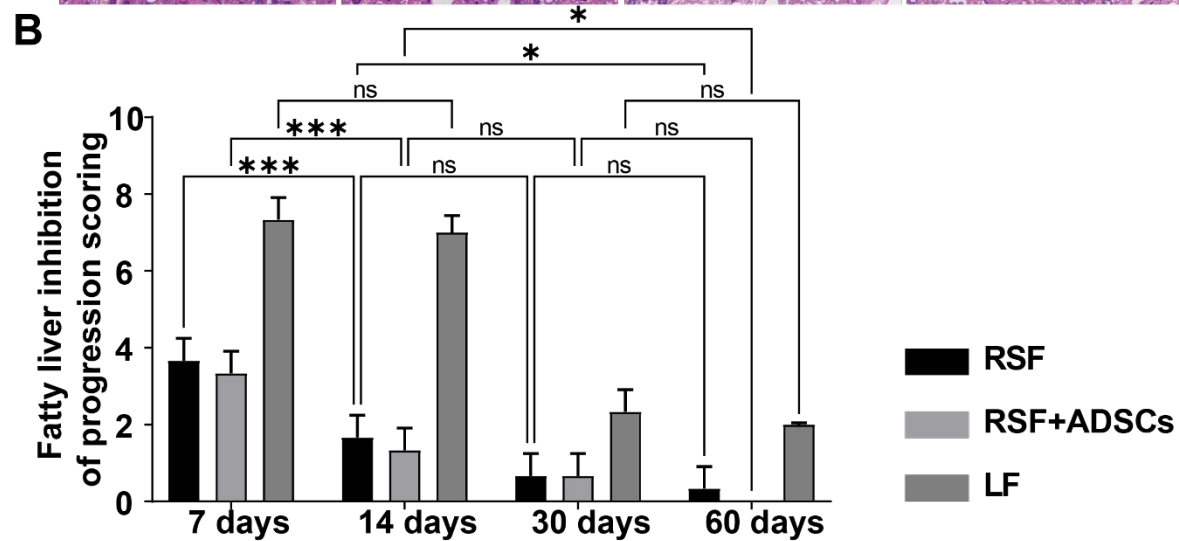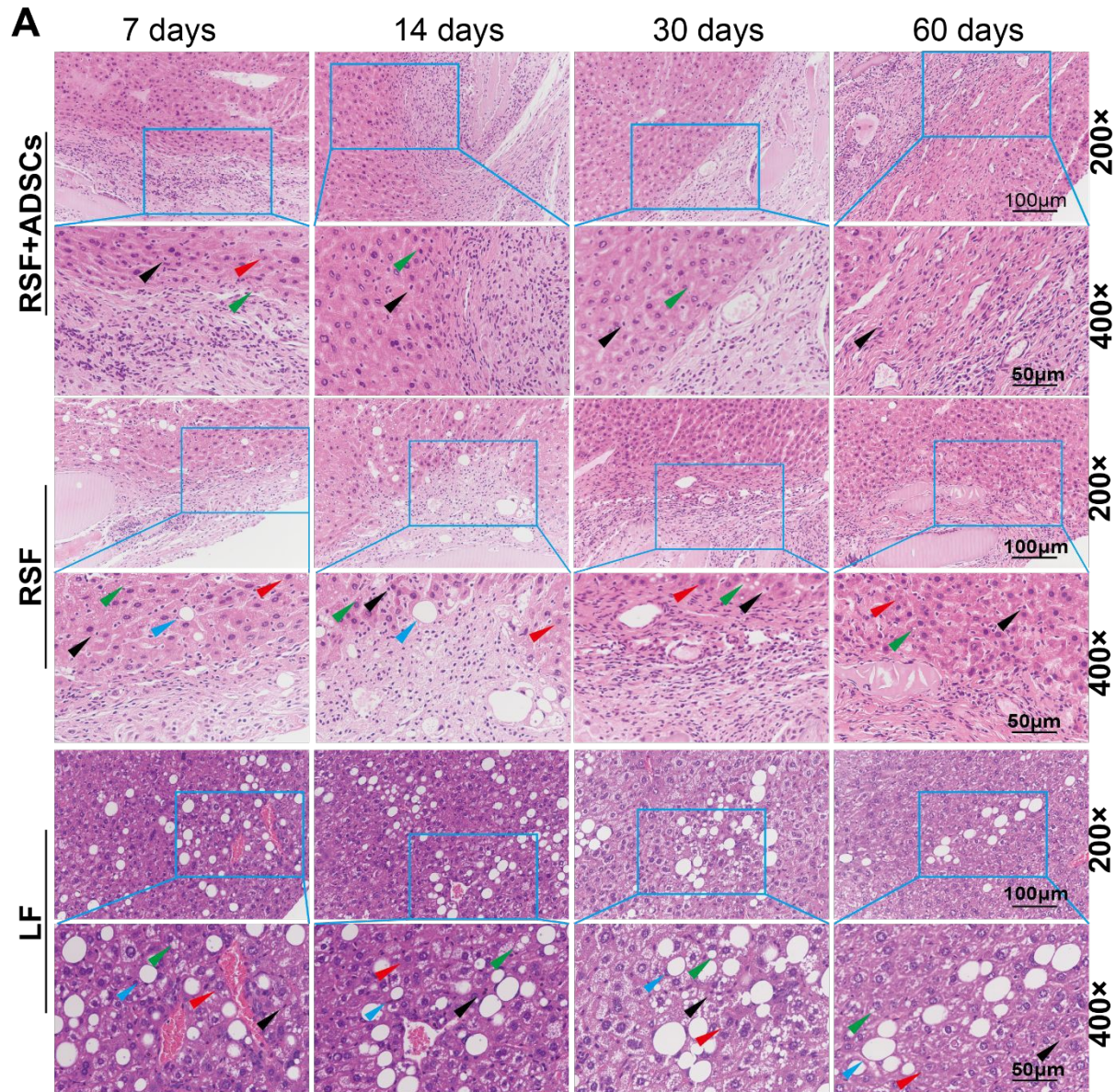
207 **Fig.2. HE staining of mouse livers after transplantation of materials. A)** HE staining of mouse

208 livers at 7, 14, 30, and 60 days post-transplantation in each group (green arrows: fatty degeneration

209 of hepatocytes; red arrows: hydropic degeneration of hepatocytes; black arrows: inflammatory

210 cells; blue arrows: macrovesicular steatosis). B) Semi-quantitative analysis of HE staining. Data

211 are presented as mean ± SD. Statistical analysis: $*p < 0.05$, $**p < 0.01$, $***p < 0.001$, ns: not

212 significant.

213 HE staining showed that the degree of injury in mice transplanted with RSF and RSF+ADSCs

214 was much weaker than that in non-transplanted injured mice (Fig. 2A). Seven days after

215 transplantation, there was still liver injury, accompanied by liver cell edema, fatty liver

216 degeneration, inflammatory cell infiltration, and cytoplasmic degeneration. On the 14th day,

217 compared with the RSF group, the RSF+ADSCs group had less large vacuolar fatty degeneration.

218 At 60 days, all experimental groups were basically recovered in terms of histology. However,

219 significant damage areas could always be observed in the LF group. These observations suggest

220 that RSF and RSF+ADSCs have similar protective effects on liver injury induced by CCl_4

221 combined with high-fat diet, but the RSF+ADSCs group has a faster repair effect than the RSF

222 group (Fig. 2B).

223

224 **3.3 Dynamics Changes of the Histopathology of Liver Fibrosis**
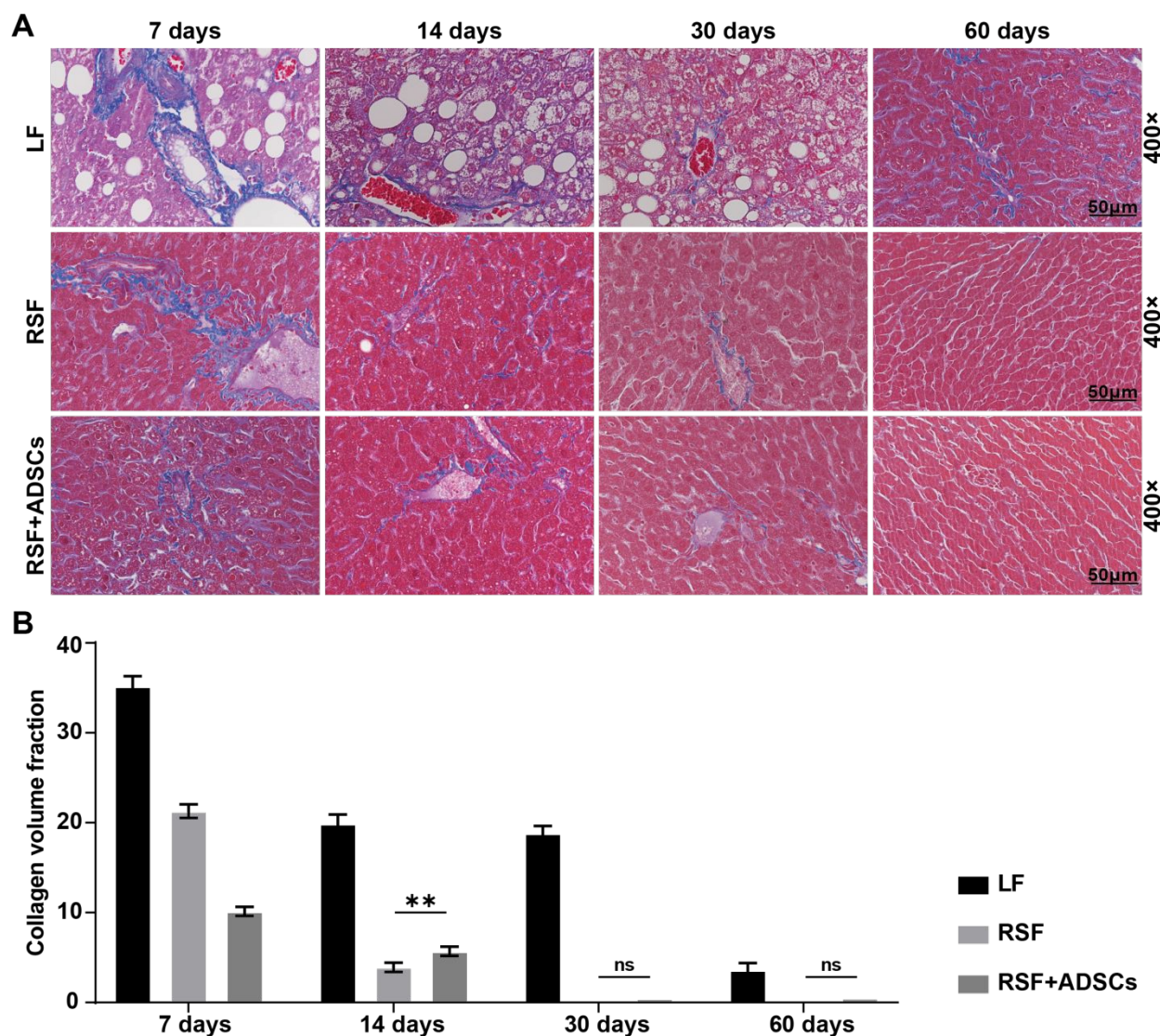
Fig.3. Masson staining and collagen area of mouse livers after transplantation materials. (A) Masson staining of mouse livers at 7, 14, 30, and 60 days post-transplantation for each group. (B) Collagen area measured from Masson staining. The data are presented as mean ± SD. Statistical analysis: $*p < 0.05$, $**p < 0.01$, $***p < 0.001$, ns: no significance.

To observe the changes in the degree of fibrosis in the liver tissue of mice after implantation, we performed Masson staining on the liver of mice at 7 days, 14 days, 30 days, and 60 days (Fig. 3A). At 7 days, results showed the presence of collagen fibers in liver tissue, indicating a high

14

233   degree of fibrosis. At 14 days, the collagen area in all experimental groups was significantly

234   reduced. At 30 days, the collagen area in the experimental group was further reduced, indicating

235   the potential of RSF implantation to improve fibrosis. At 60 days, the results of Masson staining

236   showed a significant reduction in the area of collagen fibers compared with the initial state,

237   indicating that the repair effect of RSF implantation on LF gradually increased (Fig. 3B).

238

239   **3.4 Dynamics of Liver Function and inflammatory marker CRP**

240
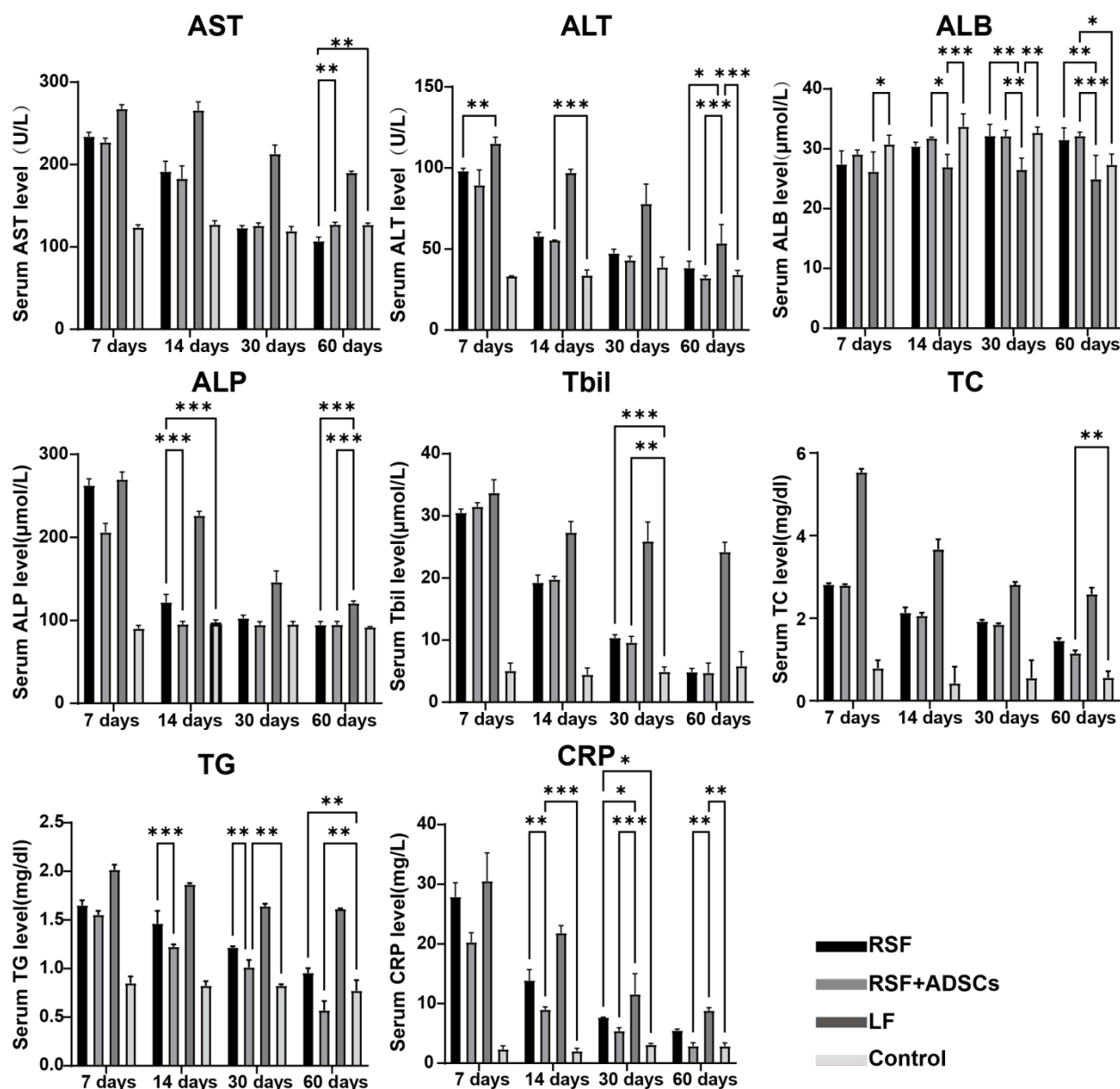
Fig.4. Analysis of liver function and inflammatory markers after RSF and RSF+ADSCs transplantation in liver fibrosis mice. Levels of AST, ALT, ALP, ALB, Tbil, TC, TG, and CRP in the plasma of each group. All data are presented as mean $\pm$ SD (n = 3). Statistical analysis was performed using t-tests: *p < 0.05, **p < 0.01, ***p < 0.001, ns: no significance.

To assess the recovery of liver function and the levels of inflammatory markers, we conducted blood biochemical analysis. The results showed that 7 days after stent transplantation, the

247   biomarker levels representing liver cell injury (AST, ALT), liver metabolic function (ALP, Tbil,

248   TC, TG), and liver inflammation (CRP) were high. The expression levels in the RSF+ADSCs

249   group were lower at different time intervals than those in the LF group and RSF group. In addition,

250   both the RSF group and the RSF+ADSCs group showed the lowest expression of liver injury and

251   inflammatory biomarkers on the 60th day (Fig. 4). Furthermore, the RSF group showed a certain

252   degree of therapeutic ability, but it was much weaker than the RSF+ADSCs group.

253

254   **3.5 Formation of new vascular and bile ducts structures in RSF scaffold**
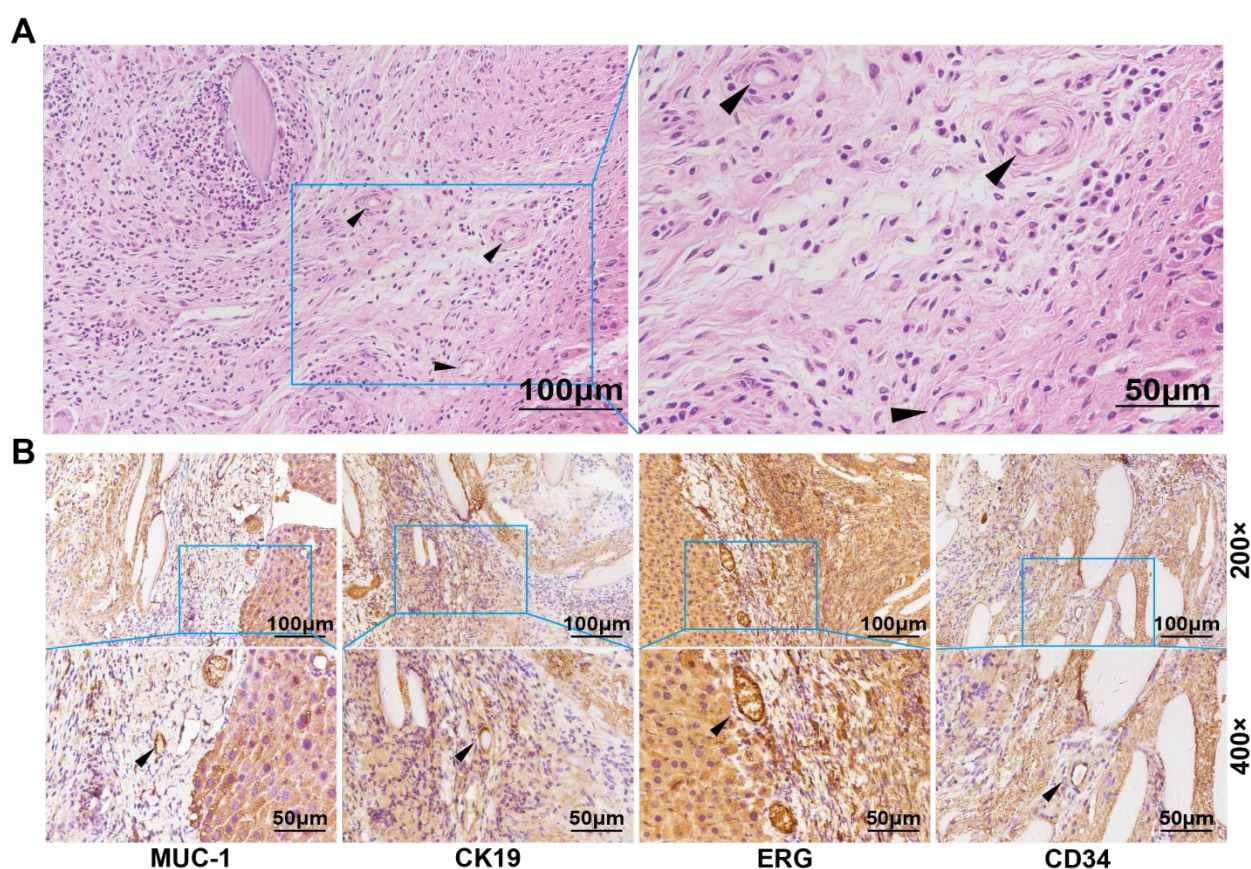
255

256   **Fig.5 Formation of new tissue on the surface of the liver after 7 days of RSF+ADSCs scaffold**

257   **transplantation.** (A)HE staining of liver vessels and bile ducts in the RSF+ADSCs group.

258 (B)Immunohistochemical staining of vascular markers CD34 and ERG, as well as bile duct

259 markers MUC-1 and CK19 in the RSF+ADSCs group (indicated by black arrows).

260   To observe the neotissue formed on the liver surface by RSF+ADSCs, we performed HE and

261 immunohistochemical staining on the neotissue 7 days after transplantation. HE staining showed

262 that tube-like structures had formed on the scaffolds in the RSF+ADSCs group (Fig. 5A).

263 Immunohistochemical staining of these tube-like structures revealed significant expression of

264 angiogenesis markers (ERG, CD34) and biliary markers (MUC1, CK19) (Fig. 5B). These results

265 suggest that RSF+ADSCs play an important role in liver regeneration and angiogenesis.

266

267 **3.6 RNA transcriptome analysis**
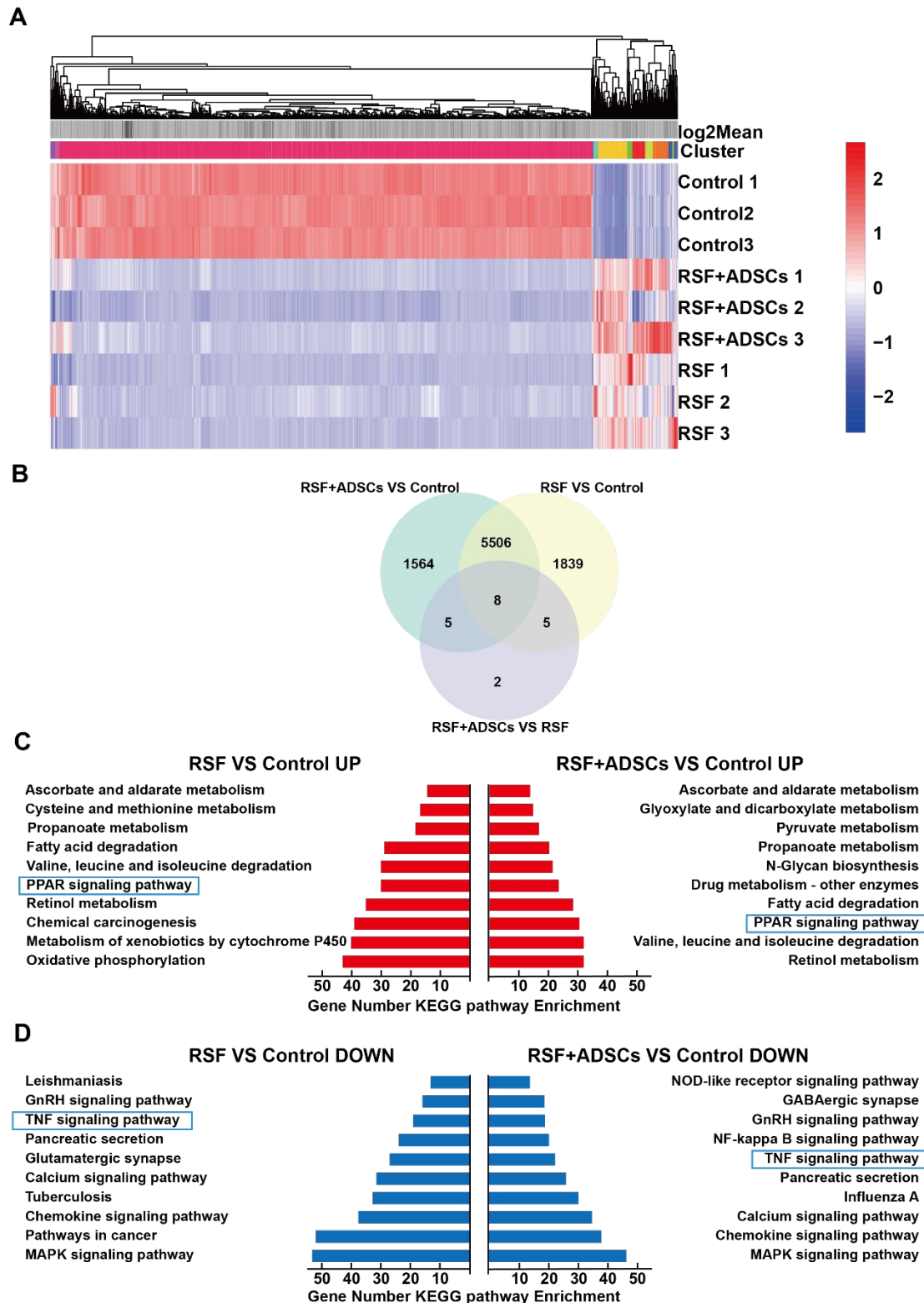
Fig.6. RNA sequencing after scaffold transplantation. (A) Cluster heatmap of differentially

expressed genes (DEG) expression. (B) Venn diagram showing the DEGs between groups. (C)

271 Upregulated pathways via KEGG pathway enrichment analysis. (D) Downregulated pathways via

272 KEGG pathway enrichment analysis.

273   To investigate the potential mechanism of RSF in repairing LF, we performed transcriptomic

274 analysis of liver tissue on the 7th day after transplantation. Cluster analysis showed that the gene

275 expression modules were similar in the RSF group and the RSF+ADSCs group, but significantly

276 different from the control group (Fig. 6A). The Venn diagram results showed that the RSF+ADSCs

277 group expressed 7,070 deferentially expressed genes, while the RSF group expressed 7,345

278 deferentially expressed genes (Fig. 6B). Through KEGG pathway enrichment analysis, compared

279 with the normal group, the RSF group and the RSF+ADSCs group significantly up-regulated cell

280 proliferation, fat degradation, redox, protein synthesis, drug metabolism and other pathways. We

281 found that both the RSF and RSF+ADSCs groups significantly up-regulated the PPAR pathway,

282 which helps maintain the balance of fat metabolism in the body by regulating fatty acid uptake,

283 synthesis, and oxidation. In addition, both the RSF and RSF+ADSCs groups significantly down-

284 regulated immune response, inflammation, and apoptosis pathways, mainly including TNF, NF-

285 kappa B signaling pathways (Fig. 6C, D).

286

287 **3.7 RSF+ADSCs Scaffolds Upregulate PPAR Signaling Pathway and Downregulate TNF**

288   **Signaling Pathway**

289
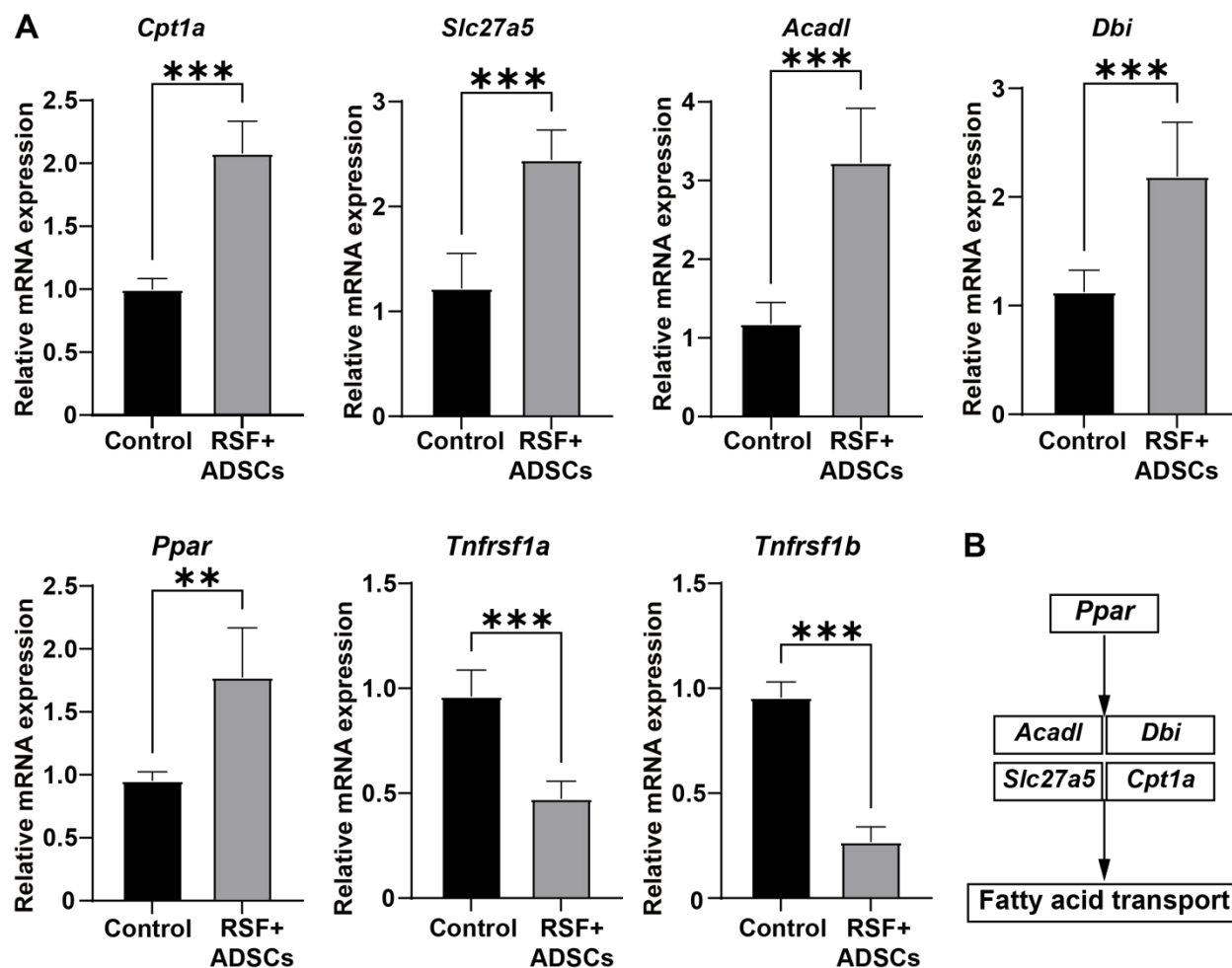
Fig.7. Genes of PPAR pathway in cavity of RSF+ADSCs were highly activated in liver fibrosis

290

mice. (A) qPCR analysis of gene expression in hepatocytes from the RSF+ADSCs group,

291

measuring *CPt1a*, *Slc27a5*, *Acadl*, *Dbi*, *Ppar*, *Tnfrsf1a* and *Tnfrsf1b*. (B) Schematic diagram of

292

the PPAR signaling pathway. The data are presented as mean ± SD. Statistical analysis: *$p < 0.05$,

293

**$p < 0.01$, ***$p < 0.001$, ns: no significance.

294

To further verify the specific mechanism of RSF+ADSCs in repairing LF, we used RT-qPCR

295

method to evaluate the gene expression of PPAR signaling pathway and TNF signaling pathway

296

in the liver tissue-scaffold connection of treated mice. The results showed that compared with the

297

Control group, the expression of *CPt1a*, *Slc27a5*, *Acadl*, *Dbi*, and *Ppar* genes in the RSF+ADSCs

298

299 group was significantly up-regulated (Fig. 7A). These genes are involved in the process of fatty

300 acid uptake, transport and oxidation. On the other hand, the expression levels of *Tnfrsf1a* and

301 *Tnfrsf1b* genes in the RSF+ADSCs group were significantly decreased, which are related to

302 inflammatory response and fibrosis. RSF+ADSCs scaffolds regulate the PPAR signaling pathway:

303 a simplified diagram (Fig. 7B). The results suggest that PPAR signaling pathway and TNF

304 signaling pathway may be involved in the fibrosis repair of LF mice after RSF+ADSCs

305 transplantation.

306

307 **4. Discussion**

308   In recent years, research on stem cells and biomaterials has provided new insights into the

309 treatment of liver fibrosis. Some clinical trial reports show that stem cells have been used to treat

310 LF, but the application of stem cells still has limitations[15]. Fortunately, our previous research has

311 indicated that biomaterials such as regenerated silk fibroin[11], apple extract[16], and nucleic acid

312 tetrahedra[17] contribute to the repair of acute liver injury. However, these materials have not yet

313 been applied to the repair of chronic liver injury.

314   In this study, we combined CCl_4 and a high-fat diet to establish a mouse model of chronic

315 liver injury. Additionally, we explored the mechanisms of liver fibrosis repair using RSF and

316 RSF+ADSCs and found that the RSF+ADSCs group had a stronger ability to repair chronic liver

317 injury than the RSF group. This group also formed a large number of new blood vessels and bile

318 ducts in the transplanted materials. Finally, we used transcriptome analysis and PCR technology

319 to validate that the expression of anti-fibrosis-related molecules in the PPAR pathway was higher

320 in the RSF+ADSCs group compared with the RSF group.

321 In this study, by combining CCl_4 with a high-fat diet, we established a mouse model of liver

322 fibrosis that closely resembles the human living environment[18, 19]. Unlike conventional non-

323 alcoholic fatty liver disease models, which are established using diets rich in fats, fructose (or

324 sucrose), and cholesterol[20, 21], our model showed late-stage histological features of liver fibrosis by

325 the 8th week, with a SAF score of 10. This model reflects both lifestyle-induced liver fibrosis and

326 drug-induced liver fibrosis[22-24], aligning with the mechanisms of liver fibrosis caused by the high-

327 paced lifestyle and drug abuse that are prevalent today.

328 The liver possesses a strong regenerative ability, which varies depending on the extent of

329 injury and its underlying cause[7]. In previous studies, various biomaterials, such as hydrogels[25];

330 polydimethylsiloxane[26, 27]; and various natural biomaterials[28], including, hyaluronic acid[29], and

331 animal extracellular matrix[30, 31], have been used, but none have been able to form liver-like tissues

332 with complex structures that include functional vascular and bile duct networks. The

333 reconstruction of complex vascular and bile duct systems remains a common challenge in tissue

334 engineering. Compared with previous studies[11], our innovation lies in the confirmation of vascular

335 and bile duct formation in the RSF+ADSCs group with the help of immunohistochemical

336 staining.

337 RSF is a natural biomaterial with good biocompatibility and biodegradability, widely used in

338 clinical applications[32, 33]. The degradation process of RSF materials is a complex biological

339 degradation process, and its properties directly affect its application in the biomedical field[34]. As a

340 natural protein-based biomaterial, the degradation of RSF primarily occurs through enzymatic

341 action, particularly by proteinase XIV, which exhibits high efficiency in degrading RSF both in

342 vivo and in vitro[35, 36]. The degradation of RSF typically begins in its hydrophilic unordered regions,

343 such as the C-terminus, N-terminus, connecting segments, and light chains, and then gradually

344 infiltrates the crystalline regions, such as the β-structured areas[37]. Finally, RSF is degraded into

345 small peptide fragments and amino acids, which are non-toxic and can be metabolized or cleared

346 by the host without accumulating in the tissue[38-40].In vivo degradation is closely related to the host

347 immune system and is primarily mediated by macrophages and foreign body giant cells (FBGCs)[41,

348 [42].It is worth noting that the degradation process of RSF materials typically does not cause

349 significant inflammation or immune reactions[43]. Its natural components (e.g., silk protein) exhibit

350 good biocompatibility, and its degradation products (e.g., peptides and amino acids) are natural

351 metabolites that will not trigger immune reactions[44].These characteristics make RSF materials

352 highly safe and reliable for clinical applications.

353 As a material with a three-dimensional spatial structure, RSF provides a microenvironment

354 for cell adhesion, proliferation, and differentiation, and also contributes to the formation of new

355 blood vessels, making it a popular material in the field of liver regeneration. In this study,

356 transcriptomic technology was used to identify that RSF scaffolds may promote protein synthesis,

357 regulate fatty acid metabolism balance, and reverse liver fibrosis by upregulating the valine,

358 leucine, and isoleucine degradation signaling pathway, the P450 signaling pathway (metabolism

359 of xenobiotics by cytochrome P450), and the PPAR signaling pathway.

360   A potential limitation of this study is the lack of a treatment group that uses ADSCs alone or

361 other materials combined with ADSCs for comparison[45]. However, ADSCs alone may not be

362 sufficient for effective liver fibrosis repair due to their inability to specifically target the fibrotic

363 area[46]. Additionally, the choice of RSF as a scaffold is based on its unique properties[47], making

364 difficult to find an equivalent control group with similar characteristics. The aim of our research

365 is to investigate whether RSF, as a carrier for stem cells, can provide an appropriate

366 microenvironment for ADSC proliferation and differentiation, and whether it has the potential to

367 promote ADSCs-mediated liver injury repair. The RSF material itself only plays an auxiliary role

368 in liver injury repair, similar to other synthetic scaffolds such as polycaprolactone[48, 49] and PEG-

369 based scaffolds[50], but these differ significantly from RSF scaffolds and are not suitable as controls.

370 Therefore, we emphasize the combination of RSF and ADSCs, investigating their combined

371 potential for promoting liver injury repair. This study focuses on exploring the mechanism of local

372 liver transplantation of regenerative biomaterials combined with stem cells for liver injury

373 repair.Future studies could explore the addition of other materials or different scaffold types to

374 further optimize the repair process.

375   To further verify the mechanism of RSF on ADSCs, this study performed transcriptomic

376 analysis between the RSF+ADSCs group and the RSF group. The results showed that the

377 RSF+ADSCs scaffold significantly upregulated the expression of genes associated with the PPAR

378 signaling pathway[51], such as *Cpt1a*, *Slc27a5*, *Acadl*, *Dbi*, and *Fabp1* (log2FC $\geq$ 2, P < 0.05).

379 PPAR[52] is a transcription factor involved in inflammation and lipid metabolism, and its activation

380 can inhibit liver fibrosis. In addition, the RSF+ADSCs scaffold can inhibit the TNF signaling

381 pathway. TNF[53]can bind to its receptors TNFR1 (Tnfrsf1a) and TNFR2 (Tnfrsf1b)[54], activating

382 downstream pathways such as NF- κ B[55], thereby triggering inflammatory responses and cell

383 apoptosis[56].

384 **5. Conclusion**

385   In summary, RSF+ADSCs have great potential in liver regeneration and LF treatment. In the

386 future, we will continue to explore the effects of RSF+ADSCs on the upstream and downstream

387 molecules of the PPAR and TNF signaling pathways in reversing liver fibrosis.

388

389   ■ **ASSOCIATED CONTENT**

390 **Supporting Information.**

391 The following files are available free of charge.

392 The sequences of the primers used (PDF)

393

394   ■ **AUTHOR INFORMATION**

395 **Corresponding Author**

396 * E-mail: yanlifmu@126.com (L.Y.).

397 * E-mail: zyp@dhu.edu.cn (Y.Z.).

398 * E-mail: wzb4000@126.com (Z.W.).

399 **Author Contributions**

400   ‡W.L. and X.S. contributed equally.

Author Contributions

402   The manuscript was written through contributions of all authors. All authors have given approval

403   to the final version of the manuscript.

404   **Weilong Li:** Writing – review & editing, Writing – original draft, Software, Methodology, Formal

405   analysis, Data curation, Conceptuali-zation. **Xiaonan Shi:** Writing – review & editing, Writing –

406   original draft, Validation, Software, Methodology, Formal analysis, Data curation,

407   Conceptualization. **Daxu Zhang:** Methodology, Formal analysis, Data curation. **Jingjing Hu:**

408   Methodology. **Shuo Zhao:** Methodology. **Shujun Ye:** Methodology. **Jingyi Wang:** Methodology.

409   **Xiaojiao Liu:** Methodology. **Qian Zhang:** Methodology. **Yaopeng Zhang:** Supervision. **Zhanbo**

410   **Wang:** Methodology, Formal analysis. Supervision. **Li Yan:** Su-pervision, Resources, Funding

411   acquisition, Conceptualization.

Funding Sources

Notes

416   The authors declare no competing financial interest.

417

418 ■ **ACKNOWLEDGEMENT**

421

422 ■ **ABBREVIATIONS**

423 RSF, Regenerated Silk Fibroin; ADSCs, Adipose-derived mesenchymal stem cells; LF, Liver

424 fibrosis; CCl_4, carbon tetrachloride; DMEM, Dulbecco's modified Eagle medium; PBS, phosphate-

425 buffered saline; FBS, fetal bovine serum; ALT, Alanine Aminotransferase; AST, Aspartate

426 Transferase; ALP, Alkaline Phosphatase; ALB, Albumin; TBIL, Total Bilirubin; TG,

427 Triglycerides; TC, Total Cholesterol; CRP, C-reactive protein; NASH, non-alcoholic

428 steatohepatitis；CPT1A, Carnitine Palmitoyltransferase 1A; SLC27A5, Solute Carrier 27A5;

429 ACADL, Acetyl-CoA Dehydrogenase Long chain; DBI, DNA-Binding Inhibitor; PPAR,

430 Peroxisome Proliferatorator-Activated Receptor; Tnfrsf1a, Tumor Necrosis Factor Superfamily

431 Member 1a; Tnfrsf1b, Tumor Necrosis Factor Superfamily Member 1b; MAPK, Mitogen-

432 Activated Protein Kinase; NF-κB, Nuclear Factor kappa B

433

434 ■ **REFERENCES**

435 1.   Cohen, J. C.;   Horton, J. D.; Hobbs, H. H., Human fatty liver disease: old questions and
436 new insights. *Science* **2011,** *332* (6037), 1519-1523.
437 2.   Angulo, P., Nonalcoholic fatty liver disease. *N Engl J Med* **2002,** *346* (16), 1221-1231.

Journal of Materials Chemistry B Accepted Manuscript

Journal of Materials Chemistry B Accepted Manuscript

438   3.   Liu, S.; Wan, H.; Yang, L.; Shen, J.; Qi, X., High prevalence of steatotic liver
439   disease and fibrosis in the general population: A large prospective study in China. *J Hepatol*
440   **2024**.

441   4.   Yang, X.; Li, Q.; Liu, W.; Zong, C.; Wei, L.; Shi, Y.; Han, Z., Mesenchymal
442   stromal cells in hepatic fibrosis/cirrhosis: from pathogenesis to treatment. *Cell Mol Immunol*
443   **2023,** *20* (6), 583-599.

444   5.   Lou, G.; Chen, Z.; Zheng, M.; Liu, Y., Mesenchymal stem cell-derived exosomes as a
445   new therapeutic strategy for liver diseases. *Exp Mol Med* **2017,** *49* (6), e346.

446   6.   Liu, P.; Mao, Y.; Xie, Y.; Wei, J.; Yao, J., Stem cells for treatment of liver
447   fibrosis/cirrhosis: clinical progress and therapeutic potential. *Stem Cell Res Ther* **2022,** *13* (1),
448   356.

449   7.   Michalopoulos, G. K.; Bhushan, B., Liver regeneration: biological and pathological
450   mechanisms and implications. *Nat Rev Gastroenterol Hepatol* **2021,** *18* (1), 40-55.

451   8.   Shi, M.; Li, Y.-Y.; Xu, R.-N.; Meng, F.-P.; Yu, S.-J.; Fu, J.-L.; Hu, J.-H.;
452   Li, J.-X.; Wang, L.-F.; Jin, L.; Wang, F.-S., Mesenchymal stem cell therapy in
453   decompensated liver cirrhosis: a long-term follow-up analysis of the randomized controlled
454   clinical trial. *Hepatol Int* **2021,** *15* (6), 1431-1441.

455   9.   Shi, M.; Zhang, Z.; Xu, R.; Lin, H.; Fu, J.; Zou, Z.; Zhang, A.; Shi, J.;
456   Chen, L.; Lv, S.; He, W.; Geng, H.; Jin, L.; Liu, Z.; Wang, F.-S., Human mesenchymal
457   stem cell transfusion is safe and improves liver function in acute-on-chronic liver failure patients.
458   *Stem Cells Transl Med* **2012,** *1* (10), 725-731.

459   10.   Guo, J.; Lin, G.-s.; Bao, C.-y.; Hu, Z.-m.; Hu, M.-y., Anti-inflammation role for
460   mesenchymal stem cells transplantation in myocardial infarction. *Inflammation* **2007,** *30* (3-4).

461   11.   Xu, L.; Wang, S.; Sui, X.; Wang, Y.; Su, Y.; Huang, L.; Zhang, Y.; Chen,
462   Z.; Chen, Q.; Du, H.; Zhang, Y.; Yan, L., Mesenchymal Stem Cell-Seeded Regenerated
463   Silk Fibroin Complex Matrices for Liver Regeneration in an Animal Model of Acute Liver
464   Failure. *ACS Appl Mater Interfaces* **2017,** *9* (17), 14716-14723.

465   12.   Chang, Q.; Yan, L.; Wang, C.-z.; Zhang, W.-h.; Hu, Y.-z.; Wu, B.-y., In vivo
466   transplantation of bone marrow mesenchymal stem cells accelerates repair of injured gastric
467   mucosa in rats. *Chin Med J (Engl)* **2012,** *125* (6), 1169-1174.

468   13.   Fan, S.; Zhang, Y.; Shao, H.; Hu, X., Electrospun regenerated silk fibroin mats with
469   enhanced mechanical properties. *Int J Biol Macromol* **2013,** *56*, 83-88.

470   14.   Ali, M.; Payne, S. L., Biomaterial-based cell delivery strategies to promote liver
471   regeneration. *Biomater Res* **2021,** *25* (1), 5.

472   15.   Yamanaka, S., Pluripotent Stem Cell-Based Cell Therapy-Promise and Challenges. *Cell
473   Stem Cell* **2020,** *27* (4), 523-531.

474   16.   Hu, J.; He, S.; Zhang, D.; Wang, Z.; Zhao, S.; Shi, X.; Li, W.; Guo, Q.;
475   Guan, W.; Yan, L., Constructing liver-like tissue in situ based on plant-derived cellulose
476   scaffolds alleviating acute liver injury. *Materials & Design* **2024,** *240*, 112856.

477   17.   Zhang, D.; Fu, L.; Yang, Y.; Guo, Q.; Hu, J.; Li, P.; Zhao, S.; Shi, X.; Li,
478   W.; Lin, Y.; Lu, W.; Yan, L., Tetrahedral framework nucleic acids improve the effectiveness

479   of adipose-derived mesenchymal stem cells in the repair of acute liver failure. *Materials Today*

480   *Nano* **2024,** *25,* 100454.

481   18.   Recena Aydos, L.;   Aparecida do Amaral, L.;   Serafim de Souza, R.;   Jacobowski, A.

482   C.;   Freitas Dos Santos, E.; Rodrigues Macedo, M. L., Nonalcoholic Fatty Liver Disease

483   Induced by High-Fat Diet in C57bl/6 Models. *Nutrients* **2019,** *11* (12).

484   19.   Hariri, N.; Thibault, L., High-fat diet-induced obesity in animal models. *Nutr Res Rev*

485   **2010,** *23* (2), 270-299.

486   20.   Farrell, G.;   Schattenberg, J. M.;   Leclercq, I.;   Yeh, M. M.;   Goldin, R.;   Teoh, N.;

487   Schuppan, D., Mouse Models of Nonalcoholic Steatohepatitis: Toward Optimization of Their

488   Relevance to Human Nonalcoholic Steatohepatitis. *Hepatology* **2019,** *69* (5), 2241-2257.

489   21.   Van Herck, M. A.;   Vonghia, L.; Francque, S. M., Animal Models of Nonalcoholic

490   Fatty Liver Disease-A Starter's Guide. *Nutrients* **2017,** *9* (10).

491   22.   Pérez Tamayo, R., Is cirrhosis of the liver experimentally produced by CCl4 and

492   adequate model of human cirrhosis? *Hepatology* **1983,** *3* (1), 112-120.

493   23.   Abraldes, J. G.;   Rodríguez-Vilarrupla, A.;   Graupera, M.;   Zafra, C.;   García-

494   Calderó, H.;   García-Pagán, J. C.; Bosch, J., Simvastatin treatment improves liver sinusoidal

495   endothelial dysfunction in CCl4 cirrhotic rats. *J Hepatol* **2007,** *46* (6), 1040-1046.

496   24.   Lee, Y.-S.; Seki, E., In Vivo and In Vitro Models to Study Liver Fibrosis: Mechanisms

497   and Limitations. *Cell Mol Gastroenterol Hepatol* **2023,** *16* (3), 355-367.

498   25.   Li, Z.;   Zhao, Y.;   Ouyang, X.;   Yang, Y.;   Chen, Y.;   Luo, Q.;   Zhang, Y.;   Zhu,

499   D.;   Yu, X.; Li, L., Biomimetic hybrid hydrogel for hemostasis, adhesion prevention and

500   promoting regeneration after partial liver resection. *Bioact Mater* **2022,** *11,* 41-51.

501   26.   Ma, P.;   Jiang, L.;   Luo, X.;   Chen, J.;   Wang, Q.;   Chen, Y.;   Ye, E.;   Loh, X. J.;

502   Wu, C.;   Wu, Y.-L.; Li, Z., Hybrid Polydimethylsiloxane (PDMS) Incorporated Thermogelling

503   System for Effective Liver Cancer Treatment. *Pharmaceutics* **2022,** *14* (12).

504   27.   Peng, J.;   Tomsia, A. P.;   Jiang, L.;   Tang, B. Z.; Cheng, Q., Stiff and tough PDMS-

505   MMT layered nanocomposites visualized by AIE luminogens. *Nat Commun* **2021,** *12* (1), 4539.

506   28.   Yuan, X.;   Wu, J.;   Sun, Z.;   Cen, J.;   Shu, Y.;   Wang, C.;   Li, H.;   Lin, D.;

507   Zhang, K.;   Wu, B.;   Dhawan, A.;   Zhang, L.; Hui, L., Preclinical efficacy and safety of

508   encapsulated proliferating human hepatocyte organoids in treating liver failure. *Cell Stem Cell*

509   **2024,** *31* (4).

510   29.   Yu, F.;   Liu, Z.;   Feng, J.;   Man, Y.;   Zhang, H.;   Shi, J.;   Pang, X.;   Yu, Y.; Bi,

511   Y., Hyaluronic acid modified extracellular vesicles targeting hepatic stellate cells to attenuate

512   hepatic fibrosis. *Eur J Pharm Sci* **2024,** *198,* 106783.

513   30.   Fan, W.;   Liu, T.;   Chen, W.;   Hammad, S.;   Longerich, T.;   Hausser, I.;   Fu, Y.;

514   Li, N.;   He, Y.;   Liu, C.;   Zhang, Y.;   Lian, Q.;   Zhao, X.;   Yan, C.;   Li, L.;   Yi, C.;

515   Ling, Z.;   Ma, L.;   Zhao, X.;   Xu, H.;   Wang, P.;   Cong, M.;   You, H.;   Liu, Z.;   Wang,

516   Y.;   Chen, J.;   Li, D.;   Hui, L.;   Dooley, S.;   Hou, J.;   Jia, J.; Sun, B., ECM1 Prevents

517   Activation of Transforming Growth Factor β, Hepatic Stellate Cells, and Fibrogenesis in Mice.

518   *Gastroenterology* **2019,** *157* (5).

519   31.   Hussein, K. H.; Park, K.-M.; Yu, L.; Kwak, H.-H.; Woo, H.-M., Decellularized
520   hepatic extracellular matrix hydrogel attenuates hepatic stellate cell activation and liver fibrosis.
521   *Mater Sci Eng C Mater Biol Appl* **2020,** *116*, 111160.

522   32.   Yao, X.; Zou, S.; Fan, S.; Niu, Q.; Zhang, Y., Bioinspired silk fibroin materials:
523   From silk building blocks extraction and reconstruction to advanced biomedical applications.
524   *Mater Today Bio* **2022,** *16*, 100381.

525   33.   Sahoo, J. K.; Hasturk, O.; Falcucci, T.; Kaplan, D. L., Silk chemistry and biomedical
526   material designs. *Nat Rev Chem* **2023,** *7* (5), 302-318.

527   34.   Guo, C.; Li, C.; Kaplan, D. L., Enzymatic Degradation of Bombyx mori Silk Materials:
528   A Review. *Biomacromolecules* **2020,** *21* (5), 1678-1686.

529   35.   Horan, R. L.; Antle, K.; Collette, A. L.; Wang, Y.; Huang, J.; Moreau, J. E.;
530   Volloch, V.; Kaplan, D. L.; Altman, G. H., In vitro degradation of silk fibroin. *Biomaterials*
531   **2005,** *26* (17), 3385-3393.

532   36.   Xiao, W.; Zhang, J.; Qu, X.; Chen, K.; Gao, H.; He, J.; Ma, T.; Li, B.; Liao,
533   X., Fabrication of protease XIV-loaded microspheres for cell spreading in silk fibroin hydrogels.
534   *J Mater Sci Mater Med* **2020,** *31* (12), 128.

535   37.   Wang, H.-Y.; Zhang, Y.-Q.; Wei, Z.-G., Dissolution and processing of silk fibroin for
536   materials science. *Crit Rev Biotechnol* **2021,** *41* (3), 406-424.

537   38.   Zhu, T.; Cai, G.; Zhao, W.; Yao, X.; Zhang, Y., Effects of Silk Fibroin Hydrogel
538   Degradation on the Proliferation and Chondrogenesis of Encapsulated Stem Cells.
539   *Biomacromolecules* **2025,** *26* (2), 1305-1319.

540   39.   Liu, K.; Shi, Z.; Zhang, S.; Zhou, Z.; Sun, L.; Xu, T.; Zhang, Y.; Zhang, G.;
541   Li, X.; Chen, L.; Mao, Y.; Tao, T. H., A Silk Cranial Fixation System for Neurosurgery.
542   *Adv. Healthcare Mater.* **2018,** *7* (6), 1701359.

543   40.   Yang, X.; Li, Y.; Liu, X.; Zhang, R.; Feng, Q., In Vitro Uptake of Hydroxyapatite
544   Nanoparticles and Their Effect on Osteogenic Differentiation of Human Mesenchymal Stem
545   Cells. *Stem Cells Int.* **2018,** *2018* (1), 1.

546   41.   Lu, Q.; Hu, X.; Wang, X.; Kluge, J. A.; Lu, S.; Cebe, P.; Kaplan, D. L., Water-
547   insoluble silk films with silk I structure. *Acta Biomater* **2010,** *6* (4), 1380-1387.

548   42.   Hu, X.; Shmelev, K.; Sun, L.; Gil, E.-S.; Park, S.-H.; Cebe, P.; Kaplan, D. L.,
549   Regulation of silk material structure by temperature-controlled water vapor annealing.
550   *Biomacromolecules* **2011,** *12* (5), 1686-1696.

551   43.   Zhu, J.; Du, Y.; Backman, L. J.; Chen, J.; Ouyang, H.; Zhang, W., Cellular
552   Interactions and Biological Effects of Silk Fibroin: Implications for Tissue Engineering and
553   Regenerative Medicine. *Small (Weinheim an Der Bergstrasse, Germany)* **2025,** *21* (4),
554   e2409739.

555   44.   Tian, Z.; Chen, H.; Zhao, P., Compliant immune response of silk-based biomaterials
556   broadens application in wound treatment. *Frontiers in Pharmacology* **2025,** *16*.

557   45.   Hu, C.; Zhao, L.; Li, L., Current understanding of adipose-derived mesenchymal stem
558   cell-based therapies in liver diseases. *Stem Cell Res Ther* **2019,** *10* (1), 199.

Journal of Materials Chemistry B Accepted Manuscript

559 46.   He, Y.; Guo, X.; Lan, T.; Xia, J.; Wang, J.; Li, B.; Peng, C.; Chen, Y.; Hu,
560 X.; Meng, Z., Human umbilical cord-derived mesenchymal stem cells improve the function of
561 liver in rats with acute-on-chronic liver failure via downregulating Notch and Stat1/Stat3
562 signaling. *Stem Cell Res Ther* 2021, *12* (1), 396.

563 47.   Sun, F.; Xiao, D.; Su, H.; Chen, Z.; Wang, B.; Feng, X.; Mao, Z.; Sui, X.,
564 Highly stretchable porous regenerated silk fibroin film for enhanced wound healing. *J Mater*
565 *Chem B* 2023, *11* (7), 1486-1494.

566 48.   Rahimkhoei, V.; Padervand, M.; Hedayat, M.; Seidi, F.; Dawi, E. A.; Akbari, A.,
567 Biomedical applications of electrospun polycaprolactone-based carbohydrate polymers: A
568 review. *Int J Biol Macromol* 2023, *253* (Pt 1), 126642.

569 49.   Labet, M.; Thielemans, W., Synthesis of polycaprolactone: a review. *Chem Soc Rev*
570 2009, *38* (12), 3484-3504.

571 50.   Zhu, J., Bioactive modification of poly(ethylene glycol) hydrogels for tissue engineering.
572 *Biomaterials* 2010, *31* (17), 4639-4656.

573 51.   Pawlak, M.; Lefebvre, P.; Staels, B., Molecular mechanism of PPARα action and its
574 impact on lipid metabolism, inflammation and fibrosis in non-alcoholic fatty liver disease. *J*
575 *Hepatol* 2015, *62* (3), 720-733.

576 52.   Francque, S.; Verrijken, A.; Caron, S.; Prawitt, J.; Paumelle, R.; Derudas, B.;
577 Lefebvre, P.; Taskinen, M.-R.; Van Hul, W.; Mertens, I.; Hubens, G.; Van Marck, E.;
578 Michielsen, P.; Van Gaal, L.; Staels, B., PPARα gene expression correlates with severity and
579 histological treatment response in patients with non-alcoholic steatohepatitis. *J Hepatol* 2015, *63*
580 (1), 164-173.

581 53.   Tilg, H.; Diehl, A. M., Cytokines in alcoholic and nonalcoholic steatohepatitis. *N Engl J*
582 *Med* 2000, *343* (20), 1467-1476.

583 54.   Wullaert, A.; van Loo, G.; Heyninck, K.; Beyaert, R., Hepatic tumor necrosis factor
584 signaling and nuclear factor-kappaB: effects on liver homeostasis and beyond. *Endocr Rev* 2007,
585 *28* (4), 365-386.

586 55.   Ding, W.-X.; Yin, X.-M., Dissection of the multiple mechanisms of TNF-alpha-induced
587 apoptosis in liver injury. *J Cell Mol Med* 2004, *8* (4), 445-454.

588 56.   Broen, J. C. A.; van Laar, J. M., Mycophenolate mofetil, azathioprine and tacrolimus:
589 mechanisms in rheumatology. *Nat Rev Rheumatol* 2020, *16* (3), 167-178.

590

Data availability statement

Adipose derived Mesenchymal Stem Cell-Seeded Regenerated Silk Fibroin Reverse Liver Fibrosis in Mice

Weilong Li [a, ‡], Xiaonan Shi [a, ‡], Daxu Zhang [b], Jingjing Hu [a], Shuo Zhao [a], Shujun Ye [a], Jingyi Wang [a], Xiaojiao Liu [c], Qian Zhang [d], Zhanbo Wang [e, *], Yaopeng Zhang [c, *], Li Yan [a, *]

The authors confirm that the data supporting the findings of this study are available within the article and its supplementary materials.